Multi-scale Structural Analysis of the *A*-site and Oxygen Deficient Perovskite $Sr_{11}Mo_4O_{23}$

Graham King,[1] Maxim Avdeev[2], Ilyas Qasim[3], Qingi Zhou[3], Brendan J Kennedy[3]

[1] *Lujan Neutron Scattering Center, Los Alamos National Laboratory, Los Alamos, NM, 87544, USA*

[2] *Australian Nuclear Science and Technology Organisation, Lucas Heights, NSW 2234, Australia*

[3] *School of Chemistry, The University of Sydney, Sydney, NSW 2006 Australia*

Abstract

The long range average crystal structure, as well as the short and medium range structural features, of the *A*-site deficient and oxygen deficient perovskite $Sr_{11}Mo_4O_{23}$ have been determined. Rietveld refinement of synchrotron X-ray and neutron powder diffraction data show that this compound is cubic with space group *Fd*-3*m* and a lattice parameter of a = 16.4108 Å. These findings contradict earlier reports of a tetragonal crystal structure. $Sr_{11}Mo_4O_{23}$ appears to be isostructural with $Ba_{11}W_4O_{23}$, except that the disordered coordination environment around one of the Mo sites seems to be a mixture of octahedral and square pyramidal instead of octahedral and tetrahedral. The short and medium range structural features have been inspected using the neutron pair distribution function (PDF). Short range correlations between the oxygen polyhedra surrounding the Mo(2) atom exist to avoid short O–O contacts. A model has been constructed which contains such correlations and is verified by reverse Monte Carlo (RMC) modeling of the PDF. The RMC refinements also give the distribution of inter-atomic distances in this compound which reveals how the various atomic positions are correlated and over what length scales. These results are important for understanding the ionic conduction pathways.

1. Introduction

The technological demand for materials with novel properties drives much of the current research in oxides with the ABX_3 perovskite-type structure. This is clearly demonstrated in the area of solid oxide fuel cells, where oxygen deficient perovskites are being extensively studied for their ionic conduction properties.[1-3] It is becoming apparent that simply knowing the average crystal structure is not sufficient to properly understand and model the conduction pathways in such materials and that local structural flexibility plays a critical role. Consequently, it is essential to understand the short range correlations that exist around sites of crystallographic disorder. A number of recent studies have highlighted how the actual coordination environments in oxygen deficient perovskites can be quite different from that implied by the average long range model.[4-10]

Cryolite related materials are a class of double perovskites with an A_3BX_6 formula such that one of the *B*-sites is occupied by the same element as the *A*-site (A_2ABX_6). Certain cryolite compositions which have small tolerance factors and a very large size difference between the *A* and *B* cations have been found to have highly complex crystal structures. In materials such as Sr_3WO_6 large rotations of the small BX_6 octahedra occur to give the larger *A* cation, which resides on a *B*-site, a coordination number larger than 6.[11-15] There are also oxygen deficient cryolites and related double perovskite compositions, such as $Sr_3SbO_{5.5}$, which have simple cubic crystal structures but locally have a large rearrangement of the atoms around the oxygen vacancy such that the actual coordination environments of the cations are similar to those seem in stoichiometric cryolites.[5]

There exists a small class of materials which have cryolite-like formulas but with small concentrations of vacancies on the *A*-sites and anion sites. A while ago it was realized that the cryolite related compound Ba_3WO_6 does not actually form with this composition but instead always contains some *A*-site and oxygen vacancies such that the true formula is $Ba_{11}W_4O_{23}$.[16] About a decade ago Hong was the first to fully solve the crystal structure of this compound.[17] It was found to be cubic with space group $Fd\bar{3}m$ and have a four-fold superstructure of the basic perovskite structure with a lattice parameter of a = 17.1823 Å. In this compound the *A*-site vacancies are ordered along the 110 direction. There are two distinct W atoms. The W(1) atom has an ideal octahedral coordination environment. The W(2) atom is surrounded by a disordered arrangement of 3 partially occupied oxygen sites. It is suggested that this site is octahedral ¾ of the time and tetrahedral ¼ of the time, with the tetrahedra pointing in one of four different directions. The arrangement of the oxygens atoms around the W(2) is such that it appears to give the *B*-site Ba cation an average coordination number larger than 6, which makes this structure related to other cryolite materials which have large octahedral rotations. The ionic conductivity of $Ba_{11}W_4O_{23}$ has also been measured and found to be moderate.[18]

Molybdenum containing oxygen deficient perovskites are an attractive class of materials owing to the redox activity of the Mo $5d^0$ Mo^{6+} – $5d^1$ Mo^{5+} couple, which allows electronic carriers as well. This is demonstrated by the excellent electrochemical performance of Sr_2MgMoO_{6-x} and its La doped analogs.[19,20] A Mo containing cryolite material has recently been identified as a potential ionic conductor since it was realized that it contains oxygen vacancies.

While the compound Sr_3MoO_6 has been known for a while,[21] it was recently recognized that this compound also does not actually form with this composition but instead always contains Sr and O vacancies such that the true chemical formula is $Sr_{11}Mo_4O_{23}$. Four recent studies have looked at the crystal structure of $Sr_{11}Mo_4O_{23}$ and its ionic conductivity.[22-25] The conductivity is moderate for the undoped material, but can be increased to values as high as 2.7×10^{-2} $S{\cdot}cm^{-1}$ and 1.8×10^{-2} $S{\cdot}cm^{-1}$ at 800 °C for Nb and Ti doped materials, respectively.

In this paper we examine the structure of $Sr_{11}Mo_4O_{23}$ over a wide range of length scales in order to obtain a complete picture of it. We find that the crystal structure of this material is isostructural with $Ba_{11}W_4O_{23}$, in contradiction with other recently done studies. We also look at the short range correlations that exist in the regions of crystallographic disorder so that the mechanisms of ionic conduction can be better understood.

2. Experimental

$Sr_{11}Mo_4O_{23}$ powder was synthesized by mixing stoichiometric quantities of $SrCO_3$ (Aldrich, 99.9+%) and MoO_3 (Aldrich, 99.5+%) with an agate mortar and pestle under acetone, placing the dry mixture in an alumina boat and heating at 1273 K for 12 h. Successive grinding, pelletizing, and heating were performed at 1473 K for 48 h, and finally at 1673 K, until phase pure. The sample was reground and examined by X-ray powder diffraction between heating steps using a PANalytical X'Pert PRO MPD. When synthesized $Sr_{11}Mo_4O_{23}$ has an intense yellow color.

Neutron powder diffraction data of a polycrystalline sample of $Sr_{11}Mo_4O_{23}$ were measured using the high resolution powder diffractometer Echidna at ANSTO's OPAL facility at Lucas Heights using wavelengths of 1.622 or 2.439 Å.[26] For these measurements the sample was contained in a cylindrical vanadium can. The synchrotron X-ray diffraction data were collected at ambient temperature in the angular range $5 < 2\theta < 85°$, using X-rays of wavelength 0.82706 Å on the powder diffractometer at BL-10 of the Australian Synchrotron.[27] The sample was housed in a 0.3 mm diameter capillary that was rotated during the measurements. The structures were refined using the program GSAS.[28,29] The neutron peak shape was modeled using a pseudo Voigt function and the background was estimated by interpolating between up to 40 selected points.

Neutron time-of-flight total scattering data was collected on the HIPD powder diffractometer at the Lujan Neutron Scattering Center at Los Alamos National Laboratory. The data was collected for about 20 hours to obtain excellent statistics. The pair distribution function was obtained by Fourier transforming S(Q) using a Q_{max} of 33 $Å^{-1}$ with the PDFgetN software.[30] The PDF was fit using the PDFgui and RMCProfile software.[31,32]

3. Results and Discussion

3.1 Average Structure. The first structural report of this compound was by McCarthy and Gooden who described Sr_3MoO_6 as cubic with a lattice parameter of ~16.4 Å but did not report any atomic positions.[21] Our synchrotron X-ray diffraction pattern can be indexed with this same cubic cell. This is in contrast with recent reports that have described the structure of $Sr_{11}Mo_4O_{23}$ as tetragonal. In 2014 Lopez *et al*. reported that $Sr_{11}Mo_4O_{23}$ was isostructural with $Sr_{11}Re_4O_{24}$ and concluded, based on constant wavelength neutron powder diffraction data, that it has $I4_1/a$ space group symmetry with lattice parameters of a = 11.6107 Å and c = 16.422 Å at room temperature.[22] Three later reports also looked at the high temperature behavior of this phase, Nb doped samples, and Ti doped samples.[23-25] The undoped $Sr_{11}Mo_4O_{23}$ was reported as tetragonal at all temperatures, while the doped samples were reported to be tetragonal at room temperature but transition to the cubic structure at higher temperature. We achieved a satisfactory Rietveld refinement (R_p 5.72, R_{wp} 8.66, R_F^2 14.3) using our synchrotron X-ray data with the cubic space group $Fd\bar{3}m$ and a lattice parameter of a = 16.4108 Å. While it was possible to obtain a atisfactory Rietveld fit to the present data using the tetragonal model $I4_1/a$ (which gave R_p 5.53, R_{wp} 8.49, R_F^2 13.9for the S-XRD profiles) there is no evidence from the diffraction profiles for any asymmetric broadening indicative of tetragonal symmetry and the pseudo-cubic lattice parameters, computed by dividing a by $2\sqrt{2}$ and c by 4, are essentially identical at a_{sub} = 4.1122 Å and c_{sub} = 4.1126 Å. Likewise, there is no evidence for a tetragonal distortion from a neutron diffraction pattern measured at 3 K. While the previous samples may have a different structure than ours, analysis of the tetragonal structure reported in reference 22 leads us to suspect that these samples are in fact cubic as well. The pseudo-cubic sub-cell parameters for the tetragonal structure in ref 22 are extremely similar, a_{sub} = 4.1050 Å and c_{sub} = 4.1055 Å. The lattice parameters reported at high temperature in ref 23, as well as the low temperature lattice parameters reported for the Nb and Ti doped samples reported in references 24 and 25, also have extremely similar sub-cell metrics. From this we conclude that $Sr_{11}Mo_4O_{23}$ is cubic at all temperatures and suggest that it should be reconsidered whether the doped materials are better described as cubic even at room temperature.

The cubic $Fd\bar{3}m$ structure can be considered as a four-fold superstructure of the primitive cubic perovskite structure and is the same as found in $Ba_{11}W_4O_{23}$, suggesting that these two compounds are isostructural. Therefore, the crystal structure of $Ba_{11}W_4O_{23}$ as reported by Hong was used as a starting model for a Rietveld refinement.[17] Ultimately, the refinement used a combined data set of the S-XRD data and the constant wavelength neutron powder diffraction data from Echidna to ensure good sensitivity to all elements present. The refinement converged to an excellent fit yielding accurate and precise positions of all atoms. The results of the refinement are given in Table 1 and selected bond lengths are given in Table 2. The fits to the diffraction patterns are shown in Figure 1 and the structure is shown in Figure 2. Rietveld refinements were also performed on the HIPD neutron diffraction pattern and yielded essentially identical results. A feature of the neutron diffraction profiles is the large modulations in the background, which are not apparent in the S-XRD profile, indicative of anion disorder.

An important feature of the cubic $Sr_{11}Mo_4O_{23}$ structure is a high level of disorder. The structure has three crystallographically distinct Sr cations. The Sr(1) and Sr(2) occupy 7/8 of the *A*-sites while 1/8 of these sites remain vacant. The Sr(1) cation is at an 8*b* (3/8, 3/8, 3/8) site

that comprises 1/8 of the available *A*-sites. It is surrounded by ideal MoO_6 octahedra that have no disorder of the oxygen atoms, resulting in a symmetric 12-fold coordination environment with a Sr–O(1) distance of 2.913(4) Å. Bond Valence Sum (BVS) calculations suggest that the 8*b* Sr site is significantly under-bonded, BVS = 1.4. The Sr(2) atom is at a 48*f* site and occupies ¾ of the *A*- sites. It is coordinated by both the fully occupied O(1) and partially occupied O(2) sites, giving it an average 9-fold asymmetric coordination environment with an effective average BVS of 2.1. The *A*-site vacancies are ordered along the 110 direction. The third type of Sr cation occupies a 32*e* site and forms part of the *B*-*B*' rock-salt ordered array of Sr and Mo cations. The Sr(3) atom has a 9-fold average coordination environment as a consequence of the disorder of the O(2) and O(3) oxygen surrounding it and a BVS of 1.6. The *B*'-site is occupied by two crystallographically distinct Mo atoms with equal multiplicities. The Mo(1) atom has an ideal octahedral coordination without any disorder; the Mo–O(1) distance of 1.868(3) Å is slightly shorter than optimal resulting in slight over-bonding of the Mo cation, BVS = 6.7. The Mo(2) atom is surround by 12 partially occupied oxygen sites and has an average coordination of about 5.5. The effective BVS for Mo(2), 6.7, shows that this is also over-bonded

The one key difference between the $Sr_{11}Mo_4O_{23}$ and $Ba_{11}W_4O_{23}$ structures, other than different bond distances due to different elements, involves the partially occupied oxygen sites surrounding the Mo(2)/W(2) sites. In $Ba_{11}W_4O_{23}$ there are three unique oxygen sites giving a total coordination of 18 partially occupied sites. These sites can be decomposed into an octahedron and several differently oriented tetrahedra.[17] When refining the structure of $Sr_{11}Mo_4O_{23}$ one of the three anion sites was found to have a negligible occupancy and consequently this was removed from the refinement, leaving two distinct anion sites and a total coordination of 12 partially occupied sites for Mo(2). As shown in Figure 3, four differently oriented square pyramids can be decomposed from these sites. This suggests that, unlike the 3:1 octahedral:tetrahedral coordination for W(2) in $Ba_{11}W_4O_{23}$, the Mo(2) site in $Sr_{11}Mo_4O_{23}$ has a 1:1: ratio of octahedral and square pyramidal coordination environments. It is also possible to decompose 8 differently oriented and highly distorted octahedra from these positions. In reality these octahedra are probably not as distorted as suggested by the Rietveld refinement, rather the oxygen atoms almost certainly lie at slightly different locations depending on if an octahedron or square pyramid is present. This illustrates the limits of describing the coordination around the Mo(2) by a few specific sites, as required by the Rietveld refinement. These octahedra are heavily rotated relative to their ideal orientations in the perovskite structure.

3.2 Local Structure. The pair distribution function (PDF) provides the distribution of inter-atomic distances in a material and can reveal any short range structural correlations that are present. As a first step in analyzing the local structure the experimental PDF was compared with the PDF that would be expected from the average crystal structure described in Table 1. Figure 4 shows the low-*r* fit to the experimental PDF using the structure determined from Rietveld refinement as a model. The fit is quite poor, clearly demonstrating that local deviations are present. The most likely source of these deviations is that the oxygen atoms on the partially occupied sites are not randomly distributed but their occupancies are correlated over short length scales. There are also likely cation displacements that depend on the local oxygen arrangement.

Some preliminary information about the bond distances can be deduced by simple inspection of the first few peaks in the PDF. The first peak in the PDF represents Mo–O bond distances. In $Sr_{11}Mo_4O_{23}$ most of the Mo is octahedrally coordinated while a smaller portion has either a tetrahedral or square pyramidal environment. Since the O to Mo ratio is 23:4 the two extreme cases are that ¾ of the Mo are octahedral and ¼ are square pyramidal or that 7/8 are octahedral and 1/8 are tetrahedral. Based on bond valence values, the average Mo–O bond distances for six coordinate Mo should be 1.91 Å, while it is 1.84 Å for five coordinate Mo, and 1.76 Å for four coordinate Mo. The first peak in the PDF has its greatest intensity at 1.90 Å, which is consistent with most of the Mo being octahedral. The coordination number of the remaining Mo can be determined by looking for shoulders on the low-*r* side of this peak, although the accuracy of this is limited by the low concentration of Mo with coordination less than six. With this caveat in mind, the PDF appears to have dropped to the baseline by $r = 1.76$ Å, which suggests the absence of any four coordinated Mo. Although a feature from tetrahedral Mo would be small, it should be detectable since it would be well separated from the main octahedral peak. There does appear to be a small shoulder around 1.85 Å, which could be attributed to Mo with a coordination number of five. Therefore, the shape of the first peak in the PDF suggests that half the Mo(2) sites have an octahedral coordination and the remainder have a square pyramidal coordination resulting in 3/4 of all Mo cations being six coordinate. Such a result matches the decomposition of the oxygen atom positions in the average structure, which also suggested square pyramidal coordination.

The second feature in the PDF is the peak at 2.64 Å which can be attributed to Sr–O and O–O distances. The observed peak is narrower and stronger than that calculated from the average structure model. The weakness of the calculated peak comes from the fact that there are some unrealistically short O–O distances in the average model that arise from partial occupancy of the sites. This removes some intensity from this *r*-range and makes the first peak in the PDF slightly over-fit. The next feature in the PDF runs from about 3.2 to 4.2 Å. The lower-*r* part of this feature corresponds to *A*-cation to *B*-cation distances while the higher-*r* part corresponds to *A*–*A*, *B*–*B*, and second nearest neighbor O–O distances. This feature is also poorly fit suggesting that there are cation displacements. The details of this are difficult to access just by looking at the peak but will be discussed further with the Reverse Monte Carlo (RMC) analysis. Beyond this distance all features in the PDF have contributions from all types of atom-atom pairs.

Reverse Monte Carlo modeling was used to fit the PDF. This method uses large supercells to create realistic atomic configurations and can model different length scales simultaneously within a single model. The RMC method does not accommodate fractional occupancies, so in order to generate a starting model for the refinements it is necessary to consider which of the fractionally occupied O sites will in fact be occupied. This process involved an analysis of the possible coordination environments around each atom. As noted above, there are two crystallographically unique Mo atoms in the structure. The Mo(1) atoms are always in octahedral coordination and have no oxygen disorder surrounding them. The Mo(2) atoms are surrounded by 12 partially occupied O sites and are thought to have a 1:1 mixture of five and six coordinate arrangements. There are many unrealistically short O–O distances among the 12 possible O sites surrounding the Mo(2) atom. Preventing these short O–

O distances is what drives the local order around each Mo(2), that is if a particular O site is occupied then several nearby O sites are required to be vacant as they are too close. The 12 O sites around each Mo(2) are derived from two crystallographically unique sites. Occupancy of an O(3) site precludes the occupancy of several other sites surrounding the same Mo(2) atom. Occupancy of an O(2) sites also has the same effect but also precludes the occupancy of an O(2) site surrounding an adjacent Mo(2) atom (Fig. 5). Therefore, occupancy of the O(2) sites creates a mechanism for short range correlation between the coordination environments of neighboring Mo(2) atoms.

As mentioned in section 3.1, the 12 O sites around the Mo(2) site can be decomposed into four square pyramids oriented in one of four different directions (Fig. 3). Two of these orientations have the square pyramid pointing in the direction of the chains of Mo(2) centered polyhedra. For these orientations the pyramids consist of 3 O(2) atoms and 2 O(3) atoms with an O(2) serving as the vertex. The other two possibilities have the pyramids pointing perpendicular to the chains of Mo(2) centered polyhedral. These pyramids are capped by an O(3) atom and are composed of 3 O(3) atoms and 2 O(2) atoms. A square pyramid capped by an O(3) atom can be neighbored by two other square pyramids of any orientation without there being short O–O contacts. However, if a square pyramid that is capped by an O(2) atom is present then, on the side of the vertex, it cannot have a neighbor which is a mirror image of itself as the two oxygen vertices would be too close (Fig. 6). This creates some correlation between the orientations of neighboring polyhedra, although since there are always multiple possibilities for what type of neighbor is present no long range order is driven by these considerations. As the presence of a pyramid capped by an O(2) lowers the probability of having a neighbor also capped by O(2) and the same is not true of pyramids capped by O(3), this can explain why the O(2) site was found to have a lower occupancy in the Rietveld refinement than the O(3) site. It should also be remembered that half of the polyhedra along the Mo(2) chains are octahedra. As it is possible to construct octahedra which do not contain O(2) atoms pointing along the chains, such orientations likely predominate.

In order to construct a starting model for the RMC refinements the symmetry was removed from the unit cell of the average structure and individual O(2) and O(3) sites were chosen to be occupied. In choosing which sites were occupied certain rules were developed. About half the Mo(2) were left six coordinate and about half were five coordinate. Atoms were manually moved around on octahedral sites to give the RMC simulation a reasonable starting position. The five coordinate sites were all formed as one of the square pyramids shown in Figure 3. It was made sure that no inter-polyhedral short O–O distances were present by excluding neighboring configurations that would lead to them, as outlined in Figure 6. There was a slight excess of square pyramids capped by O(3) atoms for the reason discussed above. Without violating the above listed restrictions, an attempt was made to have as broad a range of different types of neighboring polyhedra as possible. It was possible to create a large variety of local environments within a single unit cell since the unit cell is quite large. This starting model was expanded into a $4 \times 4 \times 4$ supercell containing 19,456 atoms that was used as the initial configuration for the RMC refinement. The RMC refinement was run until convergence over an *r*-range 1.72 – 26 Å. The final fit, shown in Figure 7, confirms that such an arrangement of

atoms is an accurate description of the local structure. Such a configuration, which contains a distribution of the actual coordination environments instead of average positions with fractional occupancies, can also be used as input for future calculations to more accurately model the conduction pathways.

One of the outputs generated by the RMC method is the distribution of all types of inter-atomic distances (Fig. 8). These can be examined to understand how the local structure differs from the average structure. The first peak in the PDF is now almost perfectly fit and its intensity is solely due to Mo–O bond distances. The peak of the Mo–O bond distribution is 1.89 Å and the average Mo–O bond length is 1.925 Å. This result shows that the actual Mo–O bond lengths are slightly longer than those given by the average structure and that the over-bonding of the Mo cations implied by the average structure is not real. Beyond nearest neighbor distances the Mo–O distance distribution is fairly broad, although it still has discernable peaks until ~22 Å.

The distribution of O–O distances in the refined RMC configuration lacks any of the short O–O contacts found between the sites of the crystal structure. The peak from nearest neighbor O–O distances has its greatest intensity around 2.68 Å. If this nearest neighbor peak is approximated as a Gaussian distribution it is found to have a full-width-at-half-max (FWHM) of ~0.25 Å. At longer distances the O–O distribution is nearly flat, which shows that the oxygen positions are only weakly correlated with each other beyond the nearest neighbor length scale. The distribution of Sr–O distances begins with a quite narrow nearest neighbor peak which has a FWHM of ~0.20 Å. This shows that any displacements of these atoms must be highly correlated at the nearest neighbor level. At longer length scales the Sr–O distribution is much wider and it becomes nearly flat by ~12 Å.

The cation-cation distances are also of interest. The Mo–Mo distribution consists of narrow well-defined peaks over the entire *r*-range used for the refinement. The first Mo–Mo peak has a FWHM of just 0.25 Å, which is very narrow considering that is does not occur until ~5.8 Å and these atoms are not expected to show correlated thermal motion. This shows that the Mo sub-lattice is highly regular. In contrast, the Sr–Sr distribution is quite broad even at the nearest neighbor length scale. The FWHM for the first Sr–Sr peak is roughly 0.44 Å. This shows that the Sr cations undergo local displacements which are not correlated with each other. As would be expected, the Sr–Mo distribution is of an intermediate width.

4. Conclusion

We have examined the short, medium, and long range structural features of $Sr_{11}Mo_4O_{23}$ using powder crystallography and the pair distribution function. The crystal structure of this compound is found to be cubic and isostructural with $Ba_{11}W_4O_{23}$. This assignment differs from earlier reports that the structure is tetragonal. While the crystal structure describes the oxygen atoms surrounding the Mo(2) site as a disordered array of partially occupied sites, the PDF clearly demonstrates that there is a large degree of local order. Both the crystallographic and local structure analysis suggest that the Mo(2) sites form chains thatcontain octahedral and square pyramidal coordinated Mo, which is different than what is found in $Ba_{11}W_4O_{23}$ which has

a mixture of octahedral and tetrahedral W. Avoidance of short O-O contacts is identified as the driving force for the short range order. RMC refinements confirm our proposed pattern of short range order is consistent with the PDF data and provide the distribution of inter-atomic distances. The structure has a regular array of long range ordered Mo cations. The oxygen atoms possess local order to avoid short contacts but their positions are not correlated over longer length scales. The Sr cations undergo displacements from their ideal crystallographic positions which are highly correlated with their local oxygen environment but not with each other. This information about the local arrangement of atoms provides a starting point for accurately understanding the ionic conduction which occurs along these chains.

Acknowledgements

This work has benefited from the use of HIPD at the Lujan Center of Los Alamos Neutron Science Center, funded by DOE Office of Basic Energy Sciences. Los Alamos National Laboratory is operated by Los Alamos National Security LLC under DOE Contract DE-AC52-06NA25396. This research was supported in part by the Australian Research Council and was, in part, performed at the Powder Diffraction beamline at the Australian Synchrotron.

Atom	**Wyckoff site**	***x***	***y***	***z***	**occ**	**B_{iso} (Å)**
Sr(1)	8b	3/8	3/8	3/8	1	3.51(7)
Sr(2)	48f	0.40070(5)	1/8	1/8	1	4.27(3)
Sr(3)	32e	0.22652(3)	*x*	*x*	1	4.98(4)
Mo(1)	16d	½	½	½	1	1.2832)
Mo(2)	16c	0	0	0	1	1.55(3)
O(1)	96g	0.5000(2)	*x*	0.6135(2)	1	2.29(7)
O(2)	96g	0.0837(3)	*x*	-0.0007(5)	0.369(6)	1.4(2)
O(3)	96h	0	0.0763(4)	-*y*	0.548(6)	2.2(8)

Table 1. The atomic parameters for $Sr_{11}Mo_4O_{23}$. The structure was refined in space group $Fd\bar{3}m$ using a combined S-XRD+PND data set with a lattice parameter of a = 16.449379(9) Å and the fit had a χ^2 of 2.55.

Sr(1)–O(1)	2.913(4) × 12	Sr(3)–O(1)	2.688(3) × 3
Sr(2)–O(3)	2.523(5) × 4	Sr(3)–O(3)	2.992(2) × 6
Sr(2)–O(2)	2.648(7) × 2	Mo(1)–O(1)	1.868(3) × 6

Sr(2)–O(1)	2.6326(7) × 4	Mo(2)–O(3)	1.775(9) × 6
Sr(2)–O(1)	2.913(3) × 2	Mo(2)–O(2)	1.947(7) × 6
Sr(3)–O(2)	2.580(3) × 6		

Table 2. Selected bond lengths for $Sr_{11}Mo_4O_{23}$ in Å.

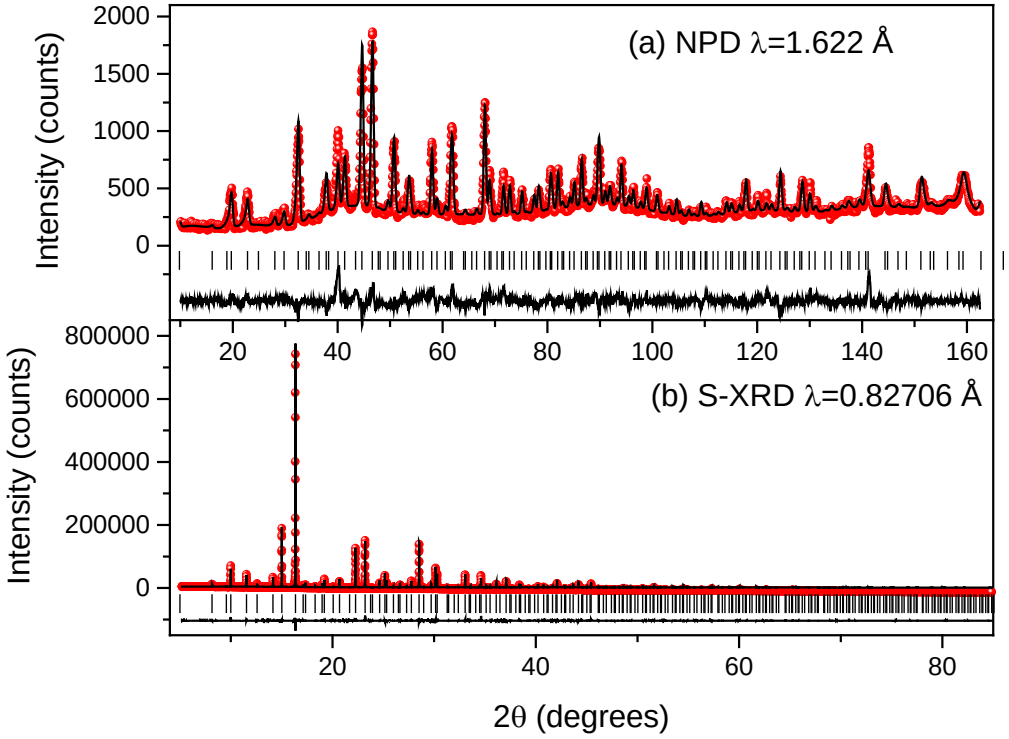

Figure 1. The fits to the synchrotron and neutron powder diffraction patterns of $Sr_{11}Mo_4O_{23}$.

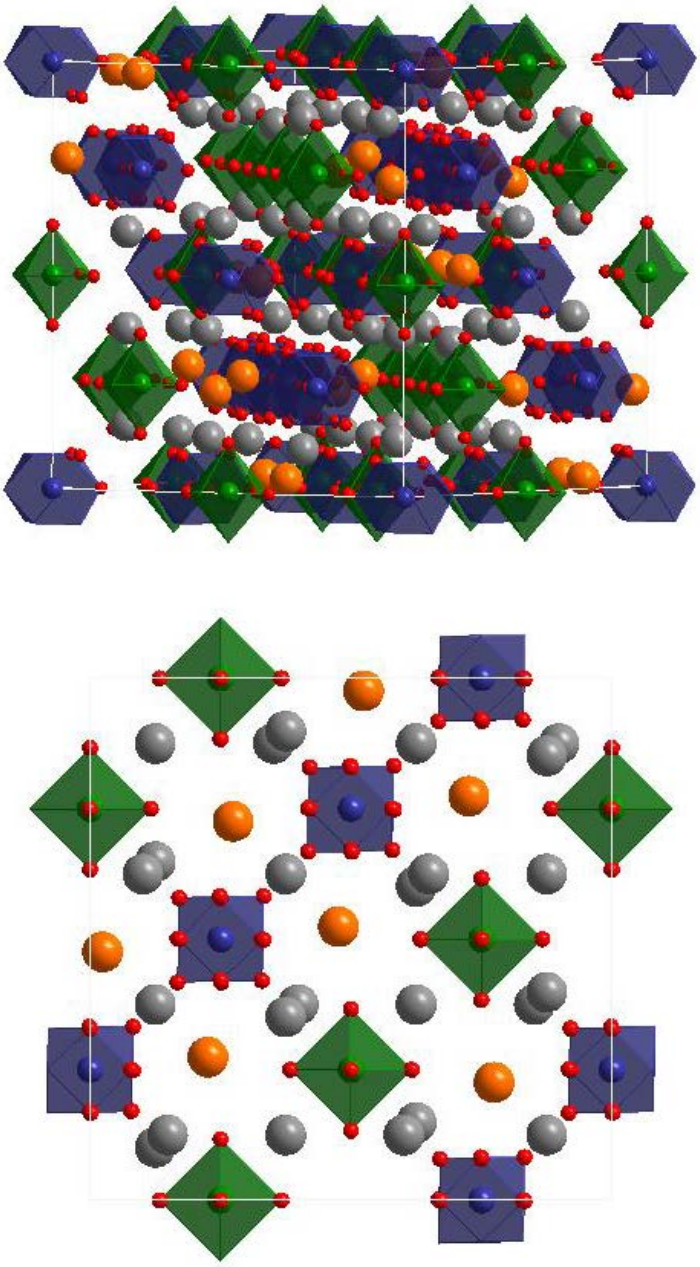

Figure 2. The crystal structure of $Sr_{11}Mo_4O_{23}$. The top view shows one unit cell while the bottom view shows one layer of polyhedra perpendicular to the [100] direction. The green atoms are the Mo(1), the blue atoms are the Mo(2), the large gray atoms are the Sr situated on the *A*-sites (the Sr(1) and Sr(2) positions), the large orange atoms are the Sr situated on the *B*-sites (Sr(3) position), and the small red atoms are the oxygen atoms. The O sites which are part of the blue Mo(2) polyhedra are about half occupied.

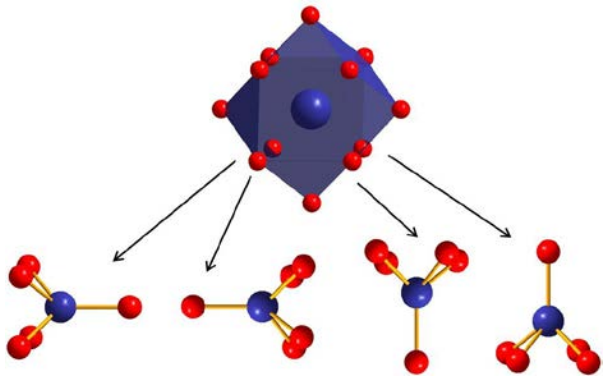

Figure 3. The coordination of O atoms (red) surrounding the Mo(2) atom (blue) and the decomposition into 4 differently oriented square pyramids. It is also possible to decompose 8 differently oriented octahedra from these positions.

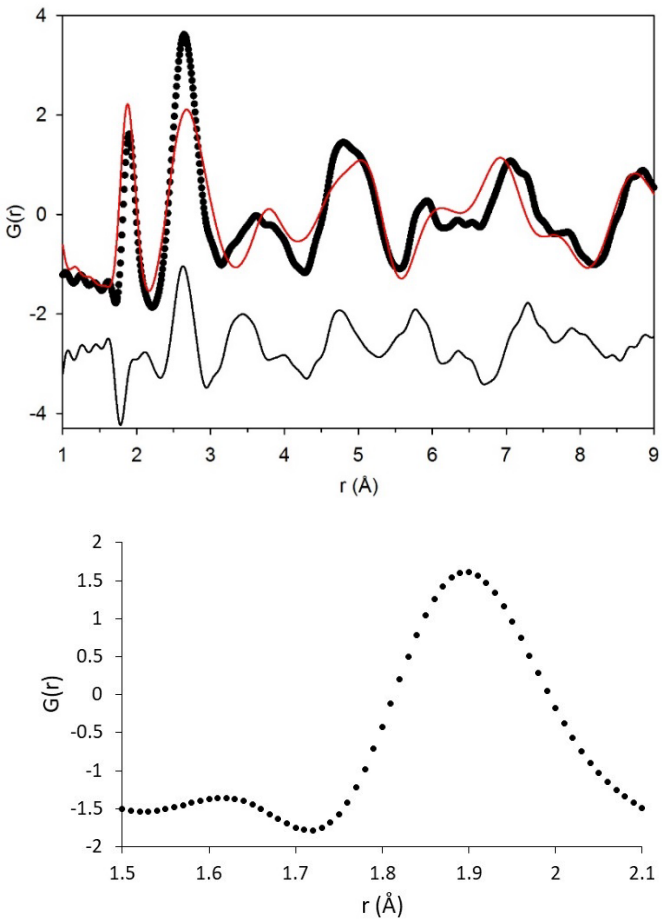

Figure 4. Top: Observed and calculated PDF for $Sr_{11}Mo_4O_{23}$. The calculated PDF was obtained using the average structure deduced from the Rietveld analysis. Bottom: Magnification of the region containing the Mo–O bond distances.

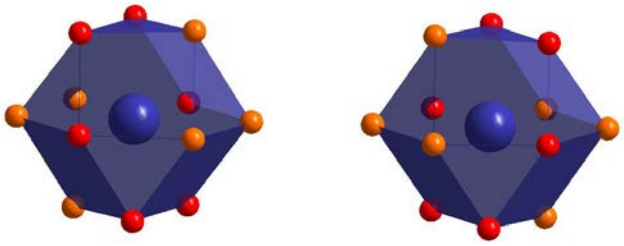

Figure 5. The coordination environment around the Mo(2) atoms (blue). The O sites are all partially occupied. The O(3) are red and the O(2) are orange. Notice how some O(2) sites (the 2 closest to the center of the figure) make a short (~1.98 Å) contact with an O(2) on an adjacent polyhedra along the chains of Mo(2) atoms.

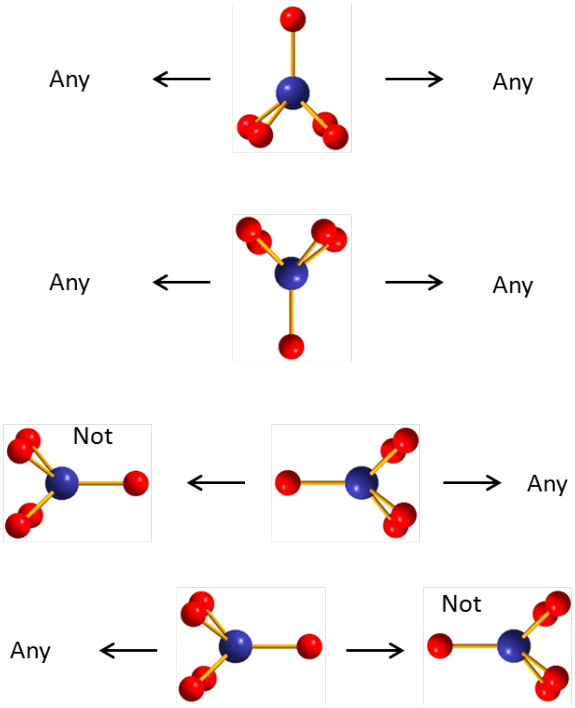

Figure 6. The allowed types of neighboring square pyramids on the two sides of a given square pyramid going along the chains of Mo(2) polyhedra.

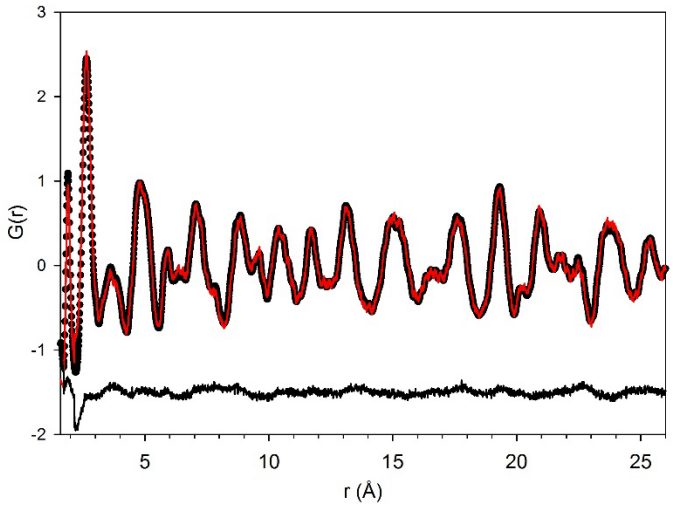

Figure 7. The fit to the PDF of $Sr_{11}Mo_4O_{23}$ using the RMC method.

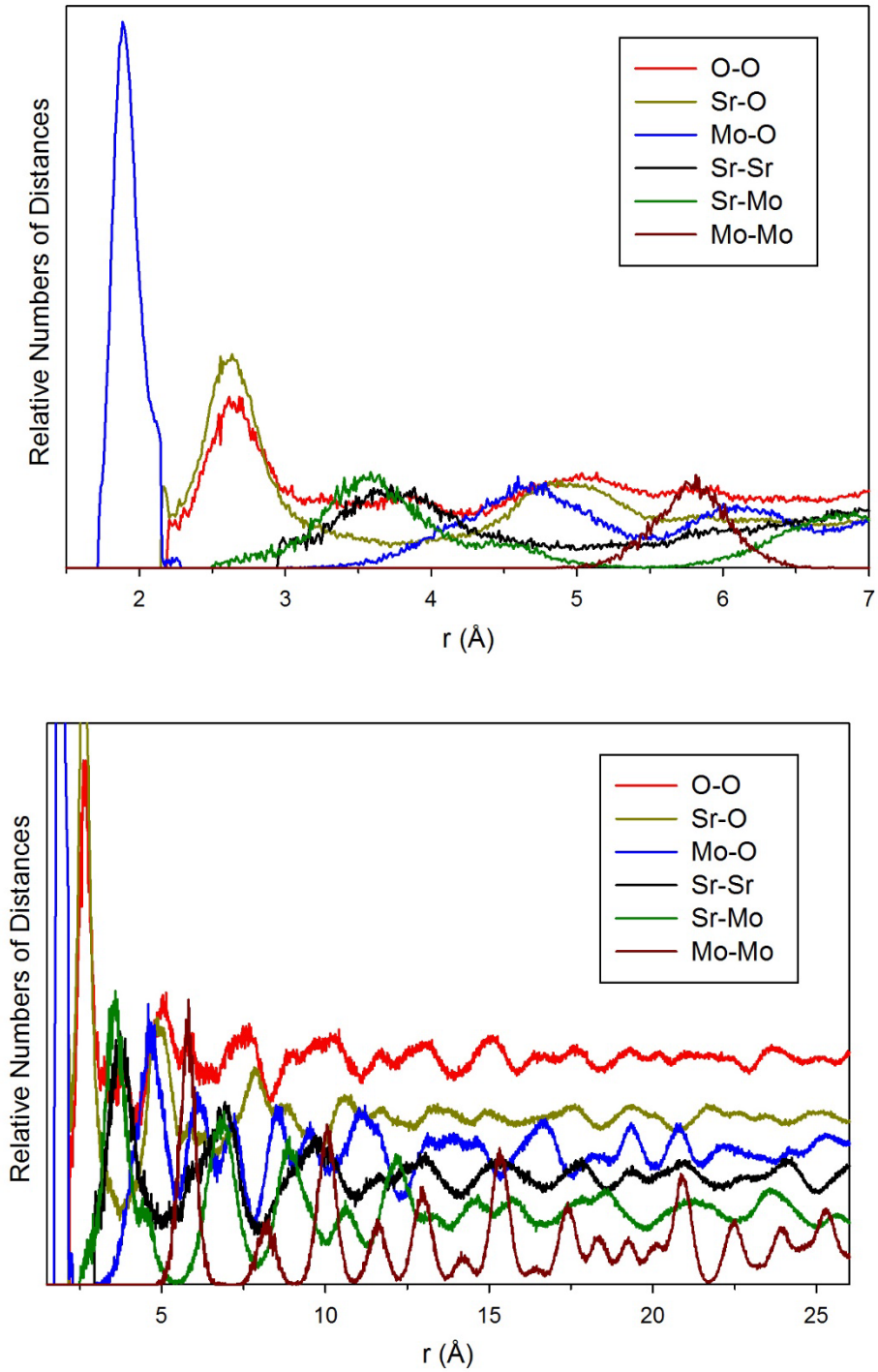

Figure 8. The bond length distributions in $Sr_{11}Mo_4O_{23}$ extracted from the RMC configuration. The top figure is a magnification of the low-*r* region. The bottom figure shows the distributions over the entire *r*-range used for the RMC refinement. In the bottom figure the tops of some of the nearest neighbor distributions have been cutoff so that the rest of the figure is of an appropriate scale.

References:

1. A. J. Jacobson, *Chem. Mater.*, 2010, **22**, 660-674.

2. A. Orera, P. R. Slater, *Chem. Mater.*, 2010, **22**, 675-690.

3. W. Zhou, J. Sunarso, M. W. Zhao, F. L. Liang, T. Klande, A. Feldhoff, *Angew. Chem. Int. Ed.*, 2013, **52,** 14036-14040.

4. F. Ramezanipour, J. E. Greedan, J. Siewenie, Th. Proffen, D. H. Ryan, A. P. Grosvenor, R. L. Donaberger, *Inorg. Chem.*, 2011, **50,** 7779–7791.

5. G. King, K. J. Thomas, A. Llobet, *Inorg. Chem*., 2012, **51,** 13060–13068.

6. F. Ramezanipour, J. E. Greedan, J. Siewenie, R. L. Donaberger, S. Turner, G. A. Botton, *Inorg. Chem*., 2012, **51,** 2638–2644.

7. F. Ramezanipour, J. E. Greedan, L. M. D. Cranswick, V. O. Garlea, J. Siewenie, G. King, A. Llobet, R. L. Donaberger, *J. Mater. Chem*., 2012, **22,** 9522–9538.

8. F. Ramezanipour, J. E. Greedan, L. M. D. Cranswick, V. O. Garlea, R. L. Donaberger, J. Siewenie, *J. Am. Chem. Soc*., 2012, **134,** 3215–3227.

9. G. King, F. Ramezanipour, A. Llobet, J. E. Greedan, *J. Solid State Chem*., 2013, **198,** 407–415.

10. G. King, C. M. Thompson, K. Luo, J. E. Greedan, M. A. Hayward. *Dalton Trans*. 2017, **46,** 1145.

11. F. J. Zuniga, A. Tressaud, J. Darriet, *J. Solid State Chem.*, 2006, **179,** 3607-3614.

12. A. M. Abakumov, G. King, V. K. Laurinavichute, M. G. Rozova, P. M. Woodward, E. V. Antipov, *Inorg. Chem.*, 2009, **48,** 9336-9344.

13. G. King, A. M. Abakumov, J. Hadermann, A. M. Alekseeva, M. G. Rozova, T. Perkisas, P. M. Woodward, G. Van Tendeloo, E. V. Antipov, *Inorg. Chem.*, 2010, **49,** 6058

14. G. King, A. M. Abakumov, P. M. Woodward, A. Llobet, A. A. Tsirlin, D. Batuk, E. V Antipov, *Inorg. Chem.*, 2011, **50,** 7792-7801.

15. A. M. Fry, P. M. Woodward, *Cryst. Growth Des.*, 2013, **13,** 5404-5410.

16. V. L. Balashov, A. A. Kharlanov, O. I. Kondratov, V. V. Fomichev, *Russ. J. Inorg. Chem.*, 1991, **36,** (1991) 254–257.

17. S.-T. Hong, *J. Solid State Chem.*, 2007, **180,** 3039-3048.

18. J.-S. Ha, E. Lee, S.-T. Hong, H.-I. Yoo, *Solid State Ionics*, 2008, **179,** 1066-1070.

19. C. Bernuy-Lopez, M. Allix, C. A. Bridges, J. B. Claridge, M. J. Rosseinsky, *Chem. Mater.*, 2007, **19,** 1035-1043.

20. Y. Jia, Y.-H. Huanga, J.-R. Yinga, J. B. Goodenough, *Electrochem. Commun.*, 2007, **9,** 1881-1885.

21. G. J. McCarthy, C. E. Gooden, *J. Inorg. Nucl. Chem.,* 1973, **35,** 2669.

22. C. A. Lopez, J. C. Pedregosa, D. G. Lamas, J. A. Alonso, *J. Appl. Cryst.* 2014, **47,** 1395–1401.

23. C. A. Lopez, J. C. Pedregosa, M. T. Fernandez-Diaz, J. A. Alonso, *J. Appl. Cryst.*, 2016, **49,** 78-84.

24. C. D. Miranda, C. A. Lopez, J. C. Pedregosa, J. A. Alonso, *Dalton Transactions*, 2017, **46,** 3934-3942.

25. C. A. Lopez, J. C. Pedregosa, M. T. Fernandez-Diaz, J. A. Alonso, *RCS Adv.*, 2017, **7,** 16163-16172.

26. K. D. Liss, B. Hunter, M. Hagen, T. Noakes, S. Kennedy, *Physica B.*, 2006, **385-86**, 1010-1012.

27. K. S. Wallwork, B. J. Kennedy, D. Wang, *AIP Conference Proceedings*, 2007, **879**, 879-882.

28. A. C. Larson, R. B. Von Dreele, Los Alamos National Laboratory Report No. LAUR 86-748, 2004

29. B. H. Toby, *J. Appl. Crystallogr.*, 2001, **34,** 210.

30. P. F. Peterson, M. Gutmann, Th. Proffen, S. J. L. Billinge, *J. Appl. Cryst.*, 2000, **33,** 1192.

31. C. L. Farrow, P. Juhas, J. W. Liu, D. Bryndin, E. S. Bozin, J. Bloch, Th. Proffen, and S. J. L. Billinge, *J. Phys.: Condens. Matter.*, 2007, **19,** 335219.

32. M. G. Tucker, D. A. Keen, M. T. Dove, A. L. Goodwin, Q. Hui, *J. Phys.: Condens. Matter.* 2007, **19,** 335218.